Robust Grid Current Control With Impedance-Phase Shaping for *LCL*-Filtered Inverters in Weak and Distorted Grid

Jinming Xu, *Member, IEEE*, Shaojun Xie, *Member, IEEE*, Binfeng Zhang, *Student Member, IEEE*, and Qiang Qian, *Student Member, IEEE*

***Abstract*—For the grid-connected *LCL*-filtered inverter, the grid current feedback active damping (AD) can assure a desirable bandwidth and a good robustness against certain parameter variations by using a minimal number of sensors. However, the inverter performance was seriously endangered by nonideal conditions at the point of common coupling (PCC), including background voltage distortions and grid impedance variation. The grid current AD could not work well for wide grid impedance variation. Hence, in this study, the robustness with such control is discussed and its relations with system parameters are derived through mathematic derivations. It is proved that, for the typical grid current AD control, a contradiction between high bandwidth and high robustness exists. On the basis of analyzing the reasons for the limitations of the typical control, a systematic approach for enhancing the robustness under complex grid conditions has been proposed. The proposed fundamental PCC voltage feedforward enhances the robustness, while the proposed phase shaping compensator assures a higher robustness with a desired bandwidth. Comparative waveforms with the typical grid current AD control have been provided to verify the correctness of the analysis and the improvement of the proposed approach.**

***Index Terms*—Grid current active damping (AD), grid distortion, grid impedance, inverter, robustness.**

I. Introduction

In DISTRIBUTED power generation systems based on renewable energies, the grid-connected inverter with an *LCL* or *LCL*-trap filter is the key interface and is widely used [1], [2]. In order to solve the serious resonance of the high-order filter, plenty of passive damping and active damping (AD) methods (including the passivity-based) have been proposed [3]–[7]. Recently, many studies paid special attention to the current control with using only one current feedback for using minimal sensors, including the delay-dependent single-loop grid current or inverter current control [8]–[12], the notch filter AD [13], [14], the grid current feedback AD [15]–[22], and the multiloop feedback through an observer to save sensors [23], [24]. Among them, the grid current feedback AD is adopted simply by a high-pass filter (HPF) with an optimal design [15] while achieving a high bandwidth and a good robustness against variations of *LCL* parameters themselves. As shown in [15] and [16], the HPF-based AD can potentially realize high bandwidth and robustness compared with the delay-dependent and notch filter ADs. Due to the above-mentioned merits over other sensorless methods, the grid current feedback AD was extensively discussed in recent two years. Studies in [17]–[22] analyzed the HPF-based grid current AD while considering the delay. For instance, the delay could considerably affect the AD performance and a double-sampling-based method was proposed for delay compensation [17], and the design of HPF parameters considering the delay was extensively discussed in [20]–[22]. It is, thus, sound to implement the HPF-based AD in different digital control systems.

But it is emphasized that the above-mentioned studies on the grid current feedback AD do not pay enough attention to the nonideal factors at the point of common coupling (PCC). Actually, the grid at the PCC is usually weak with non-negligible grid impedance [25], [26] and exhibits plenty of low-order voltage harmonics. For the existing studies on the grid current feedback AD, a small value of grid impedance was only considered in [17] and [18], and the impact of grid impedance variation was ignored in [19]–[22]. Consequently, a critical question exists, i.e., whether the inverter, especially the one using the HPF-based grid current feedback AD, can perform satisfactorily under the weak and distorted grid conditions.

In order to make the inverter perform well, the PCC voltage feedforward (PVF) and harmonic resonant (HR) controller are suggested by [2], [6], [15], and [27]–[29] to suppress low-order grid current harmonics. But, things are different if the grid impedance varies. The impedance-based modeling and the loop control modeling in [25] and [26] both found that harmonics and instabilities were aroused by large grid impedance even if the harmonic compensator was used. The study in [30] found that harmonics were aroused by the PVF in weak grid case. Then, Cespedes *et al.* [31], [32] tried some robust methods with improved feedforward or current controller to make the inverter adapt to a limited grid impedance variation, and some adaptive algorithms based on the online grid impedance estimation were

Manuscript received September 6, 2017; revised December 2, 2017 and February 5, 2018; accepted February 12, 2018. Date of publication February 21, 2018; date of current version September 28, 2018. This work was supported by the National Natural Science Foundation of China under Grant 51477077. Recommended for publication by Associate Editor Marco Liserre. *(Corresponding author: Jinming Xu.)*

The authors are with the College of Automation Engineering, Nanjing University of Aeronautics and Astronautics, Nanjing 211106, China (e-mail: xjinming01@163.com; eeac@nuaa.edu.cn; bf_zhang@nuaa.edu.cn; nuaaqianqiang@nuaa.edu.cn).

Color versions of one or more of the figures in this paper are available online at http://ieeexplore.ieee.org.

Digital Object Identifier 10.1109/TPEL.2018.2808604

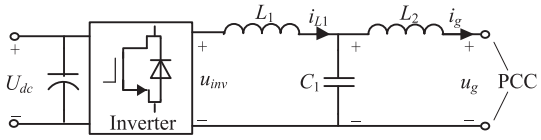

Fig. 1. Grid-connected *LCL*-filtered inverter.

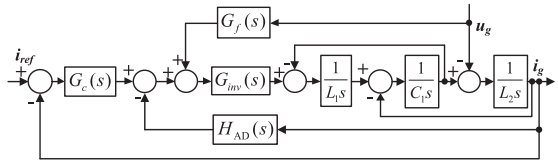

Fig. 2. Typical grid current feedback AD control structure.

proposed by Chen *et al*. [33], [34]. Note that those studies in [30]–[34] are all dedicated to the capacitor current feedback AD, which requires extra sensors. Things can be quite different once the grid current feedback AD is considered. It will be shown in this study that the grid current feedback AD encounters more difficulties in realizing a high bandwidth and robustness in the weak grid. Such AD has to be more carefully dealt with if a high robustness is expected.

In summary, it can be exciting if the inverter is properly controlled through as fewer sensors as possible. But the inverter with the grid current feedback AD (with HPF and grid current sensor only) and the harmonic compensator are challenged by the complex PCC conditions. Hence, this study is to formulate a robust grid current control plus design strategy that uses a minimal number of sensors. Contributions are 1) investigating the grid current feedback AD, through which the contradiction between high bandwidth and high robustness is found for the first time and is clearly explained; and 2) proposing a systematic approach, in which a fundamental voltage feedforward and its start-up procedure are in charge of stability and minimum start-up inrush current, and a phase shaping compensator and its design are in charge of higher robustness and desired bandwidth for different *LCL* parameters in the weak grid.

Section II briefly introduces the system descriptions and modeling. Based on clarifying the problems of the grid current feedback AD in Section III, a novel robust grid current control is proposed in Section IV and the design is proposed in Section V. Section VI shows some design examples and deals with the digital-implementation-related issues. Then, simulations and experiments are presented in Section VII. Finally, Section VIII concludes the whole paper.

II. System Descriptions and Modeling

A. Grid-Connected LCL-Filtered Inverter

In Fig. 1, the *LCL* filter includes an inverter-side inductor L_1, a capacitor C_1, and a grid-side inductor L_2. $U_{\rm dc}$ is the dc-link voltage, $u_{\rm inv}$ is the inverter output voltage, i_{L1} is the inverter-side current, i_g is the grid current, and u_g is the voltage at the PCC. Only i_g and u_g are sampled for the grid current control and phase-locked loop (PLL).

The *LCL*-filter resonance frequency is

$$f_{\rm res} = \frac{\omega_{\rm res}}{2\pi} = \frac{1}{2\pi}\sqrt{\frac{L_1+L_2}{L_1 L_2 C_1}}. \tag{1}$$

B. Grid Current Feedback AD

The grid current feedback AD is shown in Fig. 2, where $i_{\rm ref}$ is the grid current reference, $G_c(s)$ is the proportional-resonant (PR) controller, $G_f(s)$ is the PVF, and $H_{\rm AD}(s)$ is the HPF-based AD function

$$H_{\rm AD}(s) = -\frac{k_{\rm AD}\, s}{s+\omega_h} \tag{2}$$

where ω_h is the turnover frequency and $k_{\rm AD}$ is a positive factor. The AD parameters are

$$\begin{cases} \omega_h = 2\omega_{\rm res}\sqrt{1-k^2} \\ k_{\rm AD} = \omega_{\rm res}(L_1+L_2)\left(2-k^2\right)\sqrt{1-k^2} \end{cases} \tag{3}$$

where *k* is a positive number; here, $k = 0.85$ following [15].

Besides, $G_{\rm inv}(s)$ represents the total control delay

$$\begin{aligned} G_{\rm inv}(s) &= e^{-sT_d}\cdot\frac{1}{T_s}\cdot\frac{1-e^{-sT_s}}{s} \approx e^{-sT_d}\cdot e^{-sT_s/2} \\ &= e^{-s(T_d+T_s/2)} \end{aligned} \tag{4}$$

where T_d is the sampling and computation delay, and T_s is the sampling period. Basically, the delay with $T_d = T_s$ is not beneficial for the resonance damping, as analyzed in [7], [15]–[18], and [35]–[37] for the feedback-based ADs. In this study, the delay compensation in [35] will be applied for the grid current feedback AD, and $T_d \approx 0$, $G_{\rm inv}(s) \approx e^{-sTs/2}$.

C. Impedance-Based Stability

The impedance model is used for analyzing the robustness considering the grid impedance Z_g [26]. The ratio of Z_g and the inverter output impedance $Z_{\rm out}$ should satisfy the Nyquist criterion by counting the number of $\pm 180°$ crossings in the frequency range with gains above 0 dB [4]. Following the derivation methods in [31]–[33], $Z_{\rm out}$ is obtained as given in (5), shown at the bottom of this page.

III. Investigations of the Existing AD-Based Grid Current Feedback Control

A. Impact of Delay on Inverter Output Impedance

The effect of delay on $Z_{\rm out}$ shall be studied at first. With the use of (5) and (4), the Bode plots of $Z_{\rm out}$ with different T_d are shown in Fig. 3. The *LCL* parameters are $L_1 = 0.755$ mH,

$$Z_{\rm out} = \left.\frac{u_g}{(-i_g)}\right|_{i_{\rm ref}=0} = \frac{L_1L_2C_1s^3 + (L_1+L_2)s + G_{\rm inv}(s)H_{\rm AD}(s) + G_{\rm inv}(s)G_c(s)}{L_1C_1s^2 + 1 - G_{\rm inv}(s)G_f(s)} = \frac{N_{\rm out}(s)}{D_{\rm out}(s)} \tag{5}$$

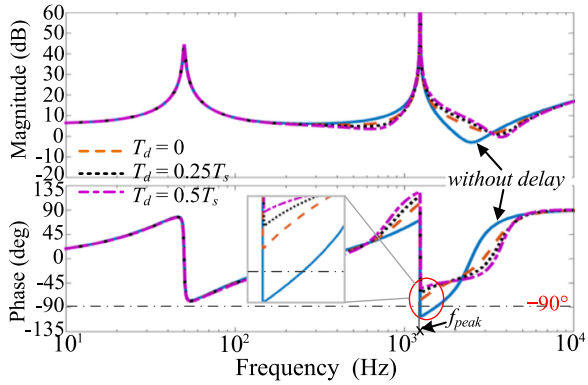

Fig. 3. Impacts of different control delays on the shaping of Z_{out}.

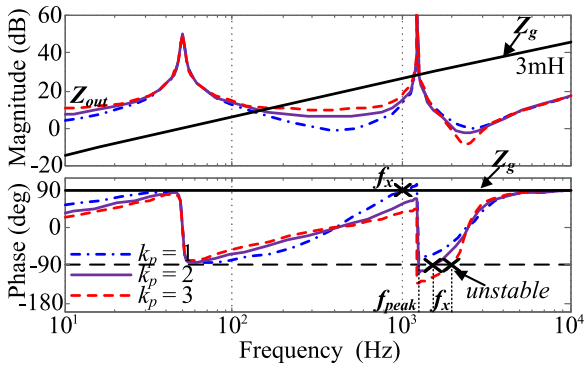

Fig. 4. Bode plots of Z_{out} with different proportional gains of $G_c(s)$.

$L_2 = 0.125\,\text{mH}$, $C_1 = 22\,\mu\text{F}$ with a switching frequency of 15 kHz, a rated power of 5 kW, and a sampling frequency of 15 kHz. It is found that the control delay has negligible effect on the magnitude and phase curves at lower frequencies, while the delay mainly affects Z_{out} around a critical frequency named f_{peak}. Seen from (5) with $G_f(s) = 0$, Z_{out} has two conjugated poles so that the magnitude curve has a peak and the phase curve decreases sharply at f_{peak}, i.e.,

$$f_{\text{peak}} = \frac{\omega_{\text{peak}}}{2\pi} = \frac{1}{2\pi\sqrt{L_1 C_1}}. \tag{6}$$

Based on the fact that the grid impedance usually behaves inductive at the relatively high frequencies [25], [26], the phases around f_{peak} can reach 90°, and thus, the stability of Z_g/Z_{out} is endangered. Note that Z_{out} without the control delay (i.e., the solid lines in Fig. 4) represents the worst case for the stability of the grid-connected inverter in the weak grid. Therefore, in the following analysis, the worst case is considered, i.e., the delay is neglected.

B. Robustness Criterion of Grid Current Feedback AD

Using (2), (3), and (5), Fig. 4 shows some Bode plots of Z_{out} with the variation of the proportional gain k_p of $G_c(s)$ while $G_f(s)$ is 0. For the present *LCL* and system parameters, a short-circuit ratio of 10 means that Z_g can reach up to 3.08 mH.

Known from Fig. 4, Z_{out} crosses 90° at the frequency f_x (i.e., 0° crossing for Z_g/Z_{out}) with a small k_p, while Z_{out} crosses −90° (i.e., 180° crossing for Z_g/Z_{out}) with a large k_p, and f_x grows with the increase in k_p. According to the Nyquist criterion, a stable system should not have the −90° crossing around f_x in the phase of Z_{out}. Note that the phase of Z_{out} crosses either 90° or −90° due to the −180° variation at f_{peak}. Therefore, the specific stability criterion for the grid current feedback AD is $f_x < f_{\text{peak}}$.

Thus, f_x should be derived. Z_{out} at f_x ($f_x \neq f_{\text{peak}}$) is expressed as

$$Z_{\text{out}\_f_x} = \frac{-jL_1L_2C_1\omega_x^3 + j(L_1+L_2)\omega_x + H_{\text{AD}}(j\omega_x) + G_c(j\omega_x)}{-L_1C_1\omega_x^2 + 1}. \tag{7}$$

Given that the phase at f_x equals 90° or −90°, Z_{out} at f_x should be a purely imaginary number, i.e.,

$$\text{Re}\{H_{\text{AD}}(j\omega_x) + G_c(j\omega_x)\} = 0. \tag{8}$$

Given that $G_c(s)$ at high frequencies can be readily seen as k_p, substituting (2) into (8) yields

$$\text{Re}\left\{-\frac{jk_{\text{AD}}\omega_x}{j\omega_x + \omega_h} + k_p\right\} = 0 \Rightarrow -\frac{k_{\text{AD}}\omega_x^2}{\omega_x^2 + \omega_h^2} + k_p = 0$$
$$\Rightarrow f_x = \frac{\omega_h}{2\pi}\sqrt{\frac{k_p}{k_{\text{AD}} - k_p}}. \tag{9}$$

Using (3), the values of f_x with $k_p = 1$, 2, 3 are separately 1.03, 1.53, 1.97 kHz, which agree well with Fig. 4 and demonstrate the correctness of the derivations. Substituting (9) into $f_x < f_{\text{peak}}$ yields the robustness criterion of the grid current feedback AD, i.e.,

$$k_p < k_{p\_\text{limit}} = \frac{\omega_{\text{peak}}^2}{\omega_{\text{peak}}^2 + \omega_h^2} k_{\text{AD}}. \tag{10}$$

C. Relation Between AD Parameters and Bandwidth

Given that the delay is ignored, the open-loop transfer function from i_{ref} to i_g in Fig. 2 (i.e., the outer loop is not closed) is

$$G^{i_g}_{i_{\text{ref}}\_\text{OL}}(s) = G_c(s) \cdot \frac{s + \omega_h}{\left[\begin{array}{l} L_1L_2C_1s^4 + L_1L_2C_1\omega_h s^3 + (L_1+L_2)s^2 + \\ (L_1+L_2)\omega_h s - k_{\text{AD}}s \end{array}\right]}. \tag{11}$$

At low frequencies, the higher-order terms in the numerator and denominator of (11) can all be ignored and $G_c(s)$ equals k_p [2], [9], [14], [33]. Then, at the 0 dB crossing frequency f_b, by using $|G^{i_g}_{i_{\text{ref}}\_\text{OL}}(j \cdot 2\pi f_b)| = 1$, it is obtained that

$$k_p = \frac{2\pi f_b\left[(L_1+L_2)\omega_h - k_{\text{AD}}\right]}{\omega_h}. \tag{12}$$

By substituting the optimal values in (3) into (12), the value of k_p subjected to a desired value of f_b, i.e., k_{p_opt}, is

$$k_{p\_\text{opt}} = \pi f_b (L_1+L_2) k^2. \tag{13}$$

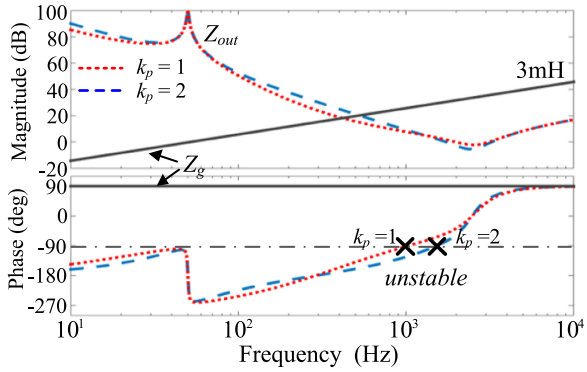

Fig. 5. Bode plots of Z_{out} with typical PCC voltage feedforward.

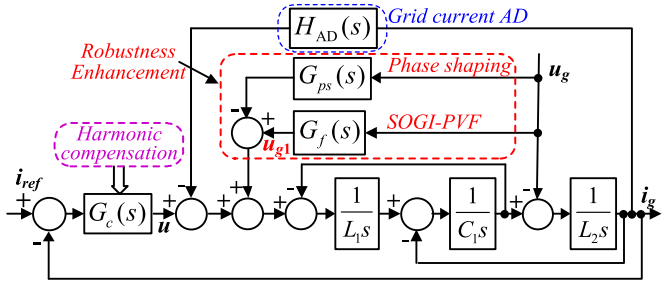

Fig. 6. Proposed robust grid current AD control with phase shaping and fundamental PVF.

D. Impact of Using PCC Voltage Feedforward

As shown in [15], [29], etc., the use of PVF can lead to a fact that the function of $G_c(s)$ is to output the reference for the voltages across the two inductors approximately. Thus, due to the reduction of control burden, using the PVF can realize high power factor and low current distortion. It is true that the two outcomes can be realized by the PR controller alternatively. But, if only the PR is used, the fast response during the inverter start-up procedure cannot be assured because the PR requires some time to establish the pulse width modulation (PWM) reference, specifically the fundamental component. In other words, the good start-up performance is another important benefit of using the PVF.

Although the PVF owns the above-mentioned merits, the performance can be affected by the grid impedance through the feedforward of the PCC voltage containing both the grid voltage and the voltage across Z_g [30]. Recall Z_{out} in (5). For Z_{out} with $G_f(s) = 1, L_1C_1s^2$ remains in the denominator so that the phases of Z_{out} below f_{peak} are much smaller than the phases of Z_{out} with $G_f(s) = 0$. Then, the phase curve of Z_{out} crosses $-90°$ (i.e., $180°$ crossing for Z_g/Z_{out}) even if the grid current feedback AD itself is robust. Fig. 5 depicts the Bode plots of Z_{out} with the PVF and grid current feedback AD fulfilling or disobeying (10) (e.g., $k_p = 1$ and $k_p = 2$). The system is unstable because of the $-90°$ crossing. Based on Fig. 5, the critical value of Z_g is calculated as 0.34 and 0.12 mH for $k_p = 1$ and 2 separately. The typical PVF is considerably harmful to the overall robustness.

E. Summary

The inverter output impedance without the control delay represents the worst case for the stability of the grid-connected inverter in the weak grid. And, if k_{p_opt} determined by (13) does not satisfy the robust criterion in (10), the grid current feedback AD cannot realize both the desired bandwidth and high robustness. Even in the case that k_{p_opt} satisfies the robust criterion, if k_{p_opt} is close to the boundary in (10), the stability margin is too small to assure a good performance. For instance, if f_b is 1 kHz, k_{p_opt} should be 2, but the robust criterion is not fulfilled; if f_b is only 0.5 kHz, k_{p_opt} is 1 fulfilling the robust criterion, but the phase at f_{peak} is very close to $-90°$, as shown in Fig. 4. It is still challenging for the grid current feedback AD to work well in the weak grid.

Moreover, if the typical PVF is adopted, the phases of the inverter output impedance can be highly reduced and the phases can intersect with $-90°$ inevitably, no matter the grid current feedback AD is robust or not. As a consequence, proper treatment should be taken in order to preserve the benefits of the PVF (e.g., good start-up performance) while guaranteeing the high robustness.

To sum up, through the theoretical analysis of the typical control in Fig. 2 in the weak grid case, two problems are clearly noticed, i.e., Problem 1: the contradiction between the desired bandwidth and the robustness, and Problem 2: the serious instability caused by the PVF.

IV. Proposed Robust AD-Based Grid Current Feedback Control

A. Fundamental PCC-Voltage Feedforward

Note that the reason for the phase reduction caused by the PVF is that $G_f(s)$ cancels the inherent term "1" in the denominator of Z_{out}. Hence, the key is to make $G_f(s)$ behave as 0 at low frequencies and this study proposes to feedforward only the fundamental content of u_g. As shown in [38] for the PLL, the second-order generalized integrator (SOGI) is capable of fundamental component extraction with no phase deviation. Thus, this study uses the SOGI as $G_f(s)$, i.e., $G_f(s)$ is

$$G_f(s) = \frac{u_{g1}}{u_g} = \frac{k_{\text{SOGI}}\omega_0 s}{s^2 + k_{\text{SOGI}}\omega_0 s + \omega_0^2} \tag{14}$$

where ω_0 is the fundamental angular frequency, k_{SOGI} is a positive number, and u_{g1} is the fundamental component of u_g. With a small k_{SOGI}, gains of $G_f(s)$ in (14) above ω_0 are treated as 0 so that phases of Z_{out} with the SOGI-PVF at low frequencies approximate to those without the PVF. That is, problem 2 can be solved. The side effect of feeding forward only u_{g1} is that magnitudes of Z_{out} at low frequencies are affected. But this side effect can be solved by adding the HR controller into $G_c(s)$.

B. Impedance-Phase Shaping Around f_{peak}

In order to solve problem 1, phases around f_{peak} should be improved. Fig. 6 shows the proposed phase shaping scheme, where $G_{ps}(s)$ is the phase shaping compensator. Z_{out}

turns to be

$$Z_{\text{out\_imp}} = \frac{L_1L_2C_1s^3 + (L_1+L_2)s + H_{\text{AD}}(s) + G_c(s)}{L_1C_1s^2 + 1 - G_f(s) + G_{ps}(s)} = \frac{N_{\text{out}}(s)}{D_{\text{out\_imp}}(s)}. \quad (15)$$

As $G_f(s)$ in (14) can be treated as 0 at the frequencies above f_0, $D_{\text{out\_imp}}$ around f_{peak} can be expressed as

$$D_{\text{out\_imp}} \approx L_1C_1s^2 + 1 + G_{ps}(s). \quad (16)$$

Therefore, in order to freely shape the phases around f_{peak}, the desired expression of $G_{ps}(s)$ is

$$G_{ps}(s) = k_{ps}s \quad (17)$$

where k_{ps} is a positive factor. Note that the derivative feedforward of the PCC voltage proposed in [6] and [29] was quite different from the proposed phase shaping compensator, although they both add an extra voltage loop into the control system. In the typical method, the first-order derivative term aims at eliminating the inherent first-order derivative term related to the capacitor current AD. Consequently, the magnitudes are shaped in order to improve the rejection of the PCC voltage-induced low-order current harmonics. The sign of the typical PVF is, thus, positive. For the proposed phase shaping $G_{ps}(s)$, the negative "feedforward" (precisely speaking, "feedback") aims at adjusting the phases around f_{peak} in order to solve the contradiction between the desired bandwidth and the robustness.

The design as well as the implementation of the digital signal processor (DSP) is detailed in Sections V and VI.

V. Proposed Design Method

A. Design and Start-Up Procedure of PCC-Voltage Feedforward

At first, $G_{ps}(s)$ is not introduced and $G_c(s)$ is treated as k_p. Fig. 7 shows some Bode plots of Z_{out} with the SOGI-PVF. Phases at low frequencies (i.e., f_0–f_{peak}) are much higher than those shown in Fig. 5, indicating a higher robustness than the PVF. Increasing k_{SOGI} leads to the phase lagging above f_0 and the phase leading around f_{peak}. The phase lagging is yielded due to the gain amplification above f_0 with larger k_{SOGI}. Besides, at f_{peak}, the denominator in (5) can be expressed as follows:

$$D_{\text{out}}(s)|_{s=j\omega_{\text{peak}}} = 0 - G_f(s)|_{s=j\omega_{\text{peak}}} = -\frac{j\omega_{\text{peak}}k_{\text{SOGI}}\omega_0}{(j\omega_{\text{peak}})^2 + j\omega_{\text{peak}}k_{\text{SOGI}}\omega_0 + \omega_0^2} \approx -\frac{j\omega_{\text{peak}}k_{\text{SOGI}}\omega_0}{(j\omega_{\text{peak}})^2} = j\frac{k_{\text{SOGI}}\omega_0}{\omega_{\text{peak}}}. \quad (18)$$

Then, $D_{\text{out}}(s)$ no longer behaves as a nondamped term at f_{peak} due to the existence of k_{SOGI}. Thus, phases of Z_{out} around f_{peak} show an increasing trend with increasing k_{SOGI}. For instance, with $k_p = 2$ [disobeying (10)], in Fig. 7(b), if k_{SOGI} increases to 1.5, the minimum phase angle around f_{peak} is a little higher than $-90°$ so that the unstable system turns stable but owns a poor margin. But, the phase lag around 100 Hz is harmful to the robustness [e.g., yielding the instability in Fig. 7(a) and the poor phase margin in Fig. 7(b)]. Hence, increasing k_{SOGI} helps to improve the stability, but the help is quite limited. That is, increasing k_{SOGI} is not a suitable choice for improving the performance no matter the robust criterion in (10) is satisfied or not.

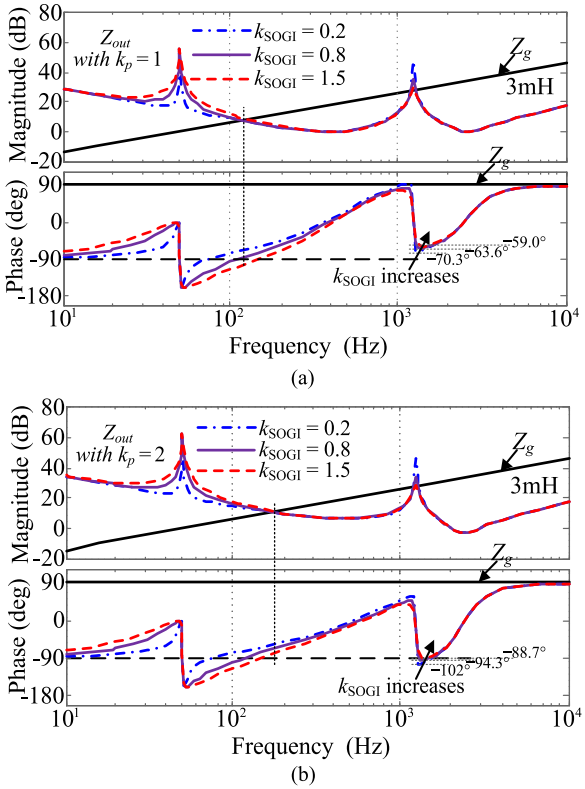

Fig. 7. Bode plots of Z_{out} with the SOGI-PVF and different k_{SOGI} with (a) $k_p = 1$ and (b) $k_p = 2$.

Hence, it is unnecessary to design a separate SOGI with an adjustable k_{SOGI} to implement the SOGI-PVF. Using the inherent u_{g1} in the SOGI-based PLL for the SOGI-PVF is applicable (here, $k_{\text{SOGI}} = 0.8$). Consequently, the start-up procedure for the SOGI-PVF is proposed. At the moment of the starting signal, the SOGI-based PLL and the sampling are enabled. After the fundamental phase of the PCC voltage is obtained, the current control plus AD algorithms and the SOGI-PVF, which uses u_{g1} as the input, are then activated at the zero crossing instant (determined by the PLL). For the sake of soft start-up, the magnitude of the grid current reference is increased gradually till it reaches the desired value.

In summary, with the SOGI-PVF, problem 2 has been solved. Besides, the merits of using the SOGI-PVF include the high power factor, the reduction of the control burden due to the high magnitude of Z_{out} at f_0, and the good start-up performance.

B. Proposed Design of an Impedance-Phase Shaping Compensator

With the proposed compensator, the inverter output impedance turns to be (15). With larger k_{ps}, the phases of

$Z_{\text{out\_imp}}$ around f_{peak} can be improved much higher because of the increased damping factor of $D_{\text{out\_imp}}$. But note that the side effect of using larger k_{ps} is that $G_{ps}(s)$ affects the magnitudes of $Z_{\text{out\_imp}}$ at a frequency below f_{peak}. As a result, the lower-frequency impedance is affected and the rejection of grid voltage deduced current harmonics can be degraded. Therefore, the design of $G_{ps}(s)$ should ensure that it has negligible or slight impact on the lower-frequency magnitudes of $Z_{\text{out\_imp}}$. Given that N_{out} has no relation with $G_{ps}(s)$, the parameter design of $G_{ps}(s)$ is equivalent to the determination of the bandwidth of $D_{\text{out\_imp}}$ in (16).

Define f_{critical} ($f_{\text{critical}} < f_{\text{peak}}$) as the critical frequency where the magnitude of the output impedance is expected to be not affected. Neglecting the slight gain of $G_f(s)$ in (14) at f_{critical}, $|D_{\text{out\_imp}}|$ in (16) is expressed as

$$\left|D_{\text{out\_imp}}\left(j2\pi f_{\text{critical}}\right)\right| = \sqrt{\left[1-L_1C_1\left(2\pi f_{\text{critical}}\right)^2\right]^2+\left(2\pi f_{\text{critical}}k_{ps}\right)^2}. \quad (19)$$

With the increase in k_{ps}, the magnitude grows. A proportional factor α is then introduced, i.e.,

$$\frac{\sqrt{\left[1-L_1C_1\left(2\pi f_{\text{critical}}\right)^2\right]^2+\left(2\pi f_{\text{critical}}k_{ps}\right)^2}}{1-L_1C_1\left(2\pi f_{\text{critical}}\right)^2}=\alpha. \quad (20)$$

Considering $Z_{\text{out}} = -u_g/i_g$, the current harmonic at f_{critical} with $G_{ps}(s)$ can be α multiplied by that without $G_{ps}(s)$. Solving (20) yields

$$k_{ps} \le k_{ps\_\text{critical}} = \frac{1-L_1C_1\left(2\pi f_{\text{critical}}\right)^2}{2\pi f_{\text{critical}}}\sqrt{\alpha^2-1}. \quad (21)$$

Fig. 8 shows the Bode plots of $Z_{\text{out\_imp}}$ with $k_p = 2$ [promising a high bandwidth but disobeying (10)]. The phase shaping improves the phase-frequency dynamic so that the phase curve around f_{peak} keeps a certain distance from the $-90°$-line. A high robustness is yielded even a high bandwidth is expected. Readers can select f_{critical} and α according to practical conditions, considering that f_{critical} relates to the frequency band of major harmonics and the selection of α should consider the limitation of current harmonics.

C. Design of a Current Controller

In addition to a PR controller, the phase-compensated HR (PC-HR) controller is recommended, i.e.,

$$G_{\text{PC-HR}}(s) = k_r\sum_{n=3,5,\ldots}^{n_{\max}}\frac{s\cos(\varphi_n)-n\omega_0\sin(\varphi_n)}{s^2+\omega_c s+(n\omega_0)^2} \quad (22)$$

where ω_c represents the bandwidth of the resonant part, k_r/ω_c is the gain at $n\omega_0$, φ_n is the leading angle for each resonant part, and $n_{\max}$ is the maximum order of harmonics to be suppressed [2], [39]. The selections of k_r and ω_c can refer to [27] and [28]. For φ_n, the selection of φ_n is done by assuming ω_c is 0, as this is the case with the lowest phase angle in the vicinity of $n\omega_0$.

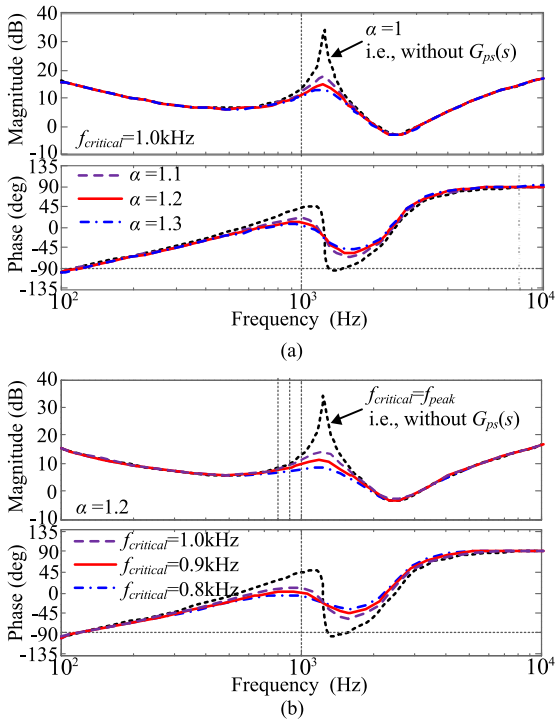

Fig. 8. Bode plots of $Z_{\text{out\_imp}}$ with the proposed control ($k_p = 2$) with (a) different α and (b) different f_{critical}.

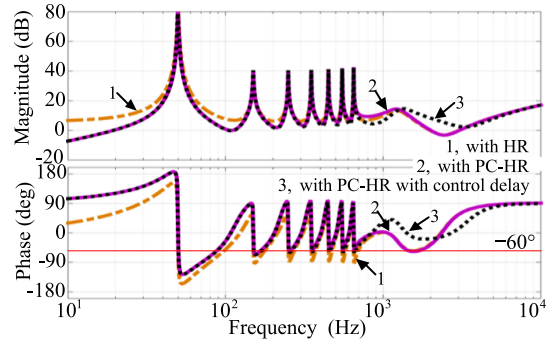

Fig. 9. Bode plots of $Z_{\text{out\_imp}}$ with different controllers.

Considering $f_0 < nf_0 < f_{\text{peak}}$ and the high gain of PC-HR at $n\omega_0$, the phase of Z_{out} with (22) in the vicinity of $n\omega_0$ is

$$\begin{aligned}\angle Z_{\text{out\_imp}}|_{s\approx jn\omega_0} &= \angle\left\{\frac{L_1L_2C_1s^3+(L_1+L_2)s+H_{\text{AD}}(s)+G_c(s)}{L_1C_1s^2+1-G_f(s)+G_{ps}(s)}\right\}\Bigg|_{s\approx jn\omega_0}\\ &\approx \angle\frac{G_{\text{PC-HR}}(s)}{k_{ps}s+1}\Bigg|_{s\approx jn\omega_0} = -\frac{\pi}{2}+\varphi_n-\arctan(n\omega_0k_{ps}).\end{aligned} \quad (23)$$

Unlike [2], an extra term exists. The objective is to increase the phases above $-\pi/2$ leaving a phase margin, named φ_{limit}. Fig. 9 shows some Bode plots of $Z_{\text{out\_imp}}$ applying (22) with $\varphi_{\text{limit}} = \pi/6, \omega_c = 6, k_r = 600$. The HR (i.e., $\varphi_n = 0$) makes the phases near $n\omega_0$ close to $-90°$. Then, harmonics near the intersecting frequency can be amplified if there are some disturbances (e.g.,

TABLE I
DESIGN RESULTS OF THE PROPOSED ROBUST CONTROL IN FIG. 6 FOR DIFFERENT *LCL* PARAMETERS

L_1 (mH)	L_2 (mH)	C_1 (μF)	f_b (kHz)	k_{p_opt}	f_{peak} (kHz)	k_{p_limit}	α	$f_{critical}$ (kHz)	$k_{ps\_critical}$	Minimum phase around f_{peak} (°)	Maximum grid impedance (mH)
							1.1	1.0	25.1μ	−63	7.3
0.755	0.125	22	1	2.00	1.23	1.38	1.2	1.0	36.3μ	−55	7.1
							1.2	0.9	55.0μ	−44	7.0
							1.1	2.0	8.8μ	8.1	8.2
0.6	0.36	8	1	2.18	2.30	3.84	1.2	2.0	12.8μ	17.4	8.1
							1.2	1.8	22.6μ	32.6	8.0
							1.1	2.0	7.1μ	2.3	10.2
0.75	0.45	6.8	1	2.72	2.23	4.66	1.2	2.0	10.3μ	10.8	10.2
							1.2	1.8	20.4μ	28.8	10.0

the step change of i_{ref}). On the contrary, the PC-HR improves the phases up to −60° and assures the robustness against the varying of Z_g.

VI. DESIGN EXAMPLES AND DISCUSSIONS

A. Design Examples

The switching and sampling frequencies are both 15 kHz and the rated power is 5 kW. Considering that the grid voltage can have harmonics up to 13th or 17th frequency, the desired f_b is 1 kHz. The controller parameters for different *LCL* parameters are presented in Table I in order to show the good applicability of the proposed control and design. The three sets of *LCL* parameters in Table I are denoted as *parameters* 1, 2, and 3 in sequence. Note that the maximum grid impedance values for the typical control in Fig. 2 in the case of $f_b = 1$ kHz are about 0.12, 0.5, and 0.6 mH for *parameters* 1, 2, and 3 separately, obtained from MATLAB analysis.

Seen from Table I, phases of Z_{out_imp} around f_{peak} are always above −90° so that the proposed robust control will not cause the system instability when Z_g increases. Moreover, in Table I, the inverter-grid system will lose the stability when Z_g increases up to the maximum grid impedance value (i.e., Z_g turns to intersect with the magnitude curve of Z_{out_imp} at the frequency where the phase is −90°). Compared with the 0.12 mH result for the typical grid current control, the robustness is highly improved. The two critical problems mentioned at the end of Section III have been solved.

Interestingly, known from Table I, a better performance is promised by *parameter* 2 or 3 with $f_b \ll f_{peak}$. That is, designing relatively large C_1 (yielding low f_{peak}) is not beneficial for the grid current feedback AD. Hence, for optimizing the performance, readers can add a specific principle, i.e., ensuring f_{peak} is much higher than f_b, when designing *LCL* parameters. Nevertheless, the proposed control can realize both desirable bandwidth and high robustness for various *LCL* parameters (even if f_{peak} is close to f_b).

B. Implementation of $G_{ps}(s)$

Generally, the pure derivative can be implemented through backward derivative and first HPF in the DSP [29], [40]. According to [40], the backward and HPF-based implementations

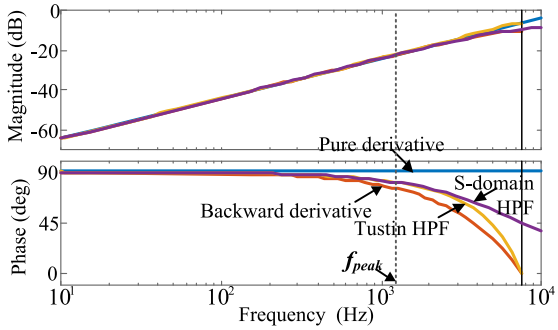

Fig. 10. Magnitude and phase characteristics of discrete derivative implementations.

are not suitable at the frequencies close to the Nyquist frequency due to the considerably mismatched phases with the pure derivative. But it is stressed that this study uses the derivative to shape the phases around f_{peak} (which is much smaller than f_{res} and Nyquist frequency). Only a small phase derivation is yielded at f_{peak}, as shown in Fig. 10. Thus, the backward and HPF-based implementations can be both applicable. Moreover, because $G_{ps}(s)$ is used to adjust the phases of Z_{out} while not to affect the magnitudes, the gain of k_{ps} is low. Seen from Fig. 10, magnitudes of all discrete derivative functions at high frequencies are kept below 0 dB. The noise interference will not be brought by the digital implementation.

C. Performance Considering the Control Delay

As discussed in Section III-A, the delay can make the phases around f_{peak} grow so that the delay is neglected to simulate the worst case in the above-mentioned analysis. With considering $G_{inv}(s)$, curve 3 in Fig. 9 shows the Bode plot of the inverter output impedance. It is found that the phases of the output impedance still keep a certain distance from −90°, indicating that the proposed robust control and design can assure a high robustness of the digitally controlled inverter in the weak grid case.

VII. VERIFICATIONS

A. Simulations

A single-phase grid-connected inverter has been built in the Saber simulator. The dc link is a voltage source set at 400 V.

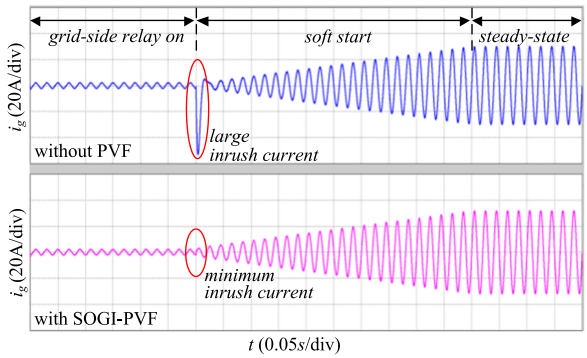

Fig. 11. Start-up waveforms of grid current without and with PVF.

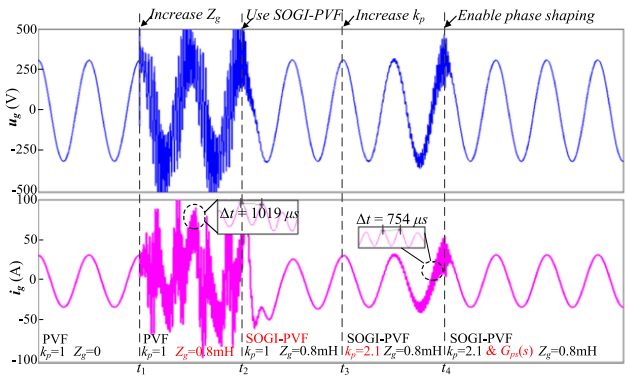

Fig. 12. Transient waveforms with the grid current AD control (before t_2, only the typical control is used).

The grid voltage is 200 V/50 Hz. The phase and amplitude of i_{ref} are given manually. The shadowed parameters in Table I are used. In the following parts, strategy 1 denotes the control in Fig. 2 and strategy 2 denotes the proposed control in Fig. 6.

At first, Fig. 11 shows the start-up grid current waveforms. As analyzed in Section III-D, at the moment of the control algorithm enabling, the PR controller requires some time to establish the PWM reference if the PVF is not used. Hence, there can be considerably large difference between u_{inv} and u_g. The large inrush current is then yielded and can cause the protection due to the over current. On the contrary, with the SOGI-PVF, u_{g1} is able to rapidly establish the PWM reference by the feedforward so that the inrush current is highly suppressed. The use of PVF is necessary even with the PR controller, and a good start-up performance is achieved by the proposed feedforward.

In addition, the simulation waveforms subjected to the grid impedance variation is shown in Fig. 12, where the effects of each part of the proposed robust grid current control can be observed. Before t_1, the inverter works well with the typical grid current AD and PVF, without the grid impedance. Once the grid impedance increases at t_1, the grid current is resonated. The harmonics around f_x (1 kHz for $k_p = 1$ in Fig. 5) are aroused. It is noticed that those harmonics disappear rapidly once the SOGI-PVF is used at t_2. In addition, as indicated in Section III, increasing k_p improves the control bandwidth but degrades the robustness. Therefore, after increasing k_p at t_3, the PCC voltage and the grid current both tend to lose the stability

TABLE II
GRID CURRENT THDS FOR DIFFERENT GRID IMPEDANCE VALUES

Z_g (mH)	0	0.12	1.0	3.1
Strategy 1	0.59%	75.8%	null	null
Strategy 2	1.13%	1.03%	1.01%	2.10%

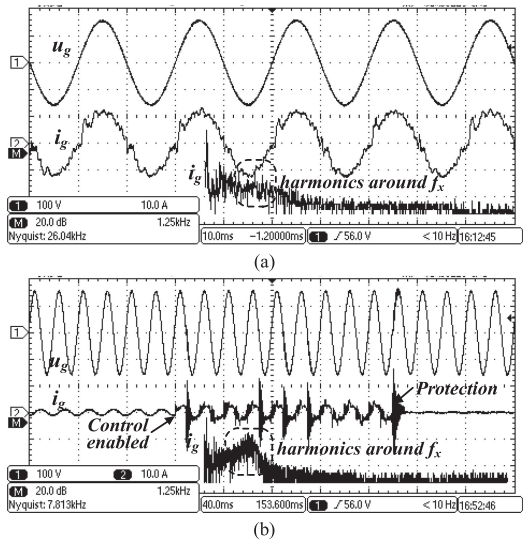

Fig. 13. Waveforms with strategy 1. (a) Inherent slight grid impedance due to wires and parasitic parameters. (b) Adding an extra 0.2 mH inductor.

and the harmonics around f_x (1.5 kHz for $k_p = 2$ in Fig. 4) are aroused. By using the proposed phase shaping compensator at t_4, those harmonics are rapidly suppressed because the phases of Z_{out} around f_{peak} are improved and the crossing with $-90°$ no longer exists. The function of the phase shaping has been confirmed. After t_4, the high bandwidth and high robustness are achieved simultaneously by the proposed robust grid current control.

At last, performances are tested while the ac grid source contains some low-order voltage harmonics (i.e., 5% 3rd, 3% 5–7th, and 2% 9–13th). In the following sections, f_b is always set at 1 kHz (i.e., $k_p = 2$). The grid current total harmonics distortion (THD) values subjected to different Z_g are presented in Table II, while the corresponding waveforms are not shown for saving pages. The THD with large Z_g for strategy 1 is not obtained because of the unstable operation. On the contrary, lower THD is achieved by the proposed strategy 2.

B. Experiments

A single-phase inverter is also built in the lab for experiments. The DSP TMS320F28035 is used to implement the sampling and the overall control. The amplitude of i_{ref} is set manually. The SOGI-PLL is used to generate the phase of i_{ref}. For the sake of safety, the experiments are tested at first in the case of a light power and 110 V/50 Hz grid.

With *parameter* 1 and strategy 1, waveforms are shown in Fig. 13. In Fig. 13(a), no extra inductor is added, while the wires and parasitic parameters act as the inherent grid impedance.

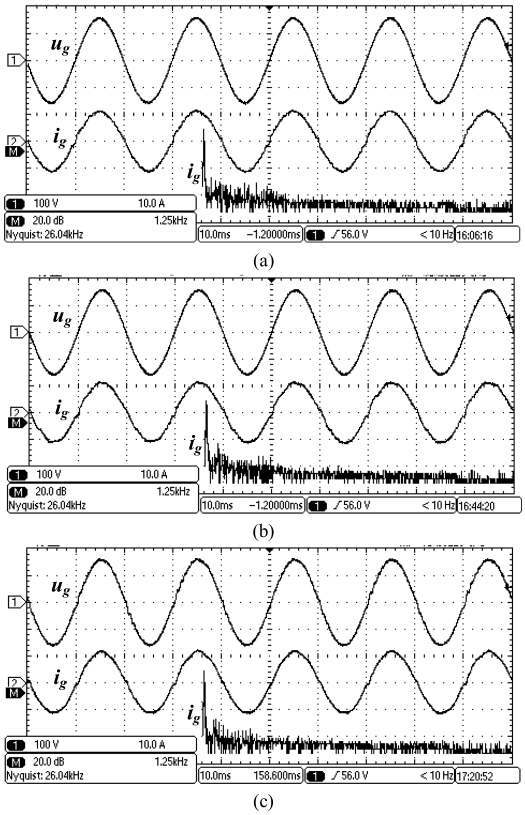

Fig. 14. Waveforms with strategy 2. (a) Inherent slight grid impedance. (b) Adding an extra 0.2 mH inductor. (c) Adding an extra 2.5 mH inductor.

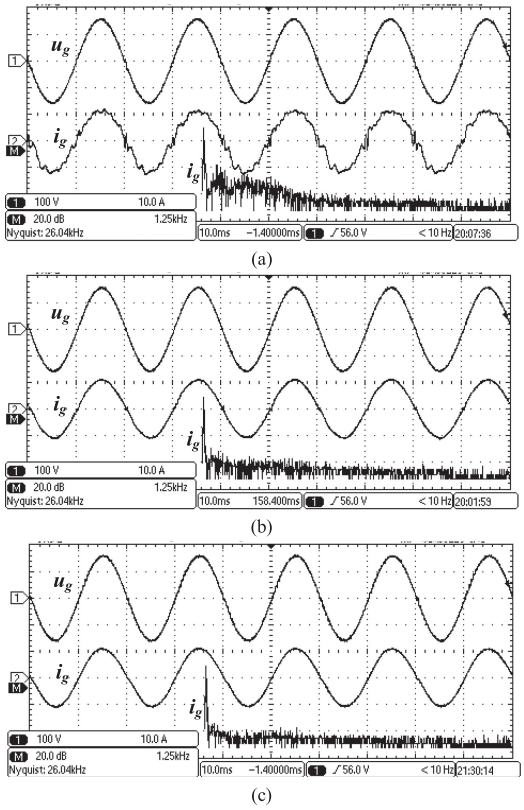

Fig. 15. Waveforms with *parameter* 2. (a) Strategy 1 and an extra 0.2 mH inductor. (b) Strategy 2 and an extra 0.2 mH inductor. (c) Strategy 2 and an extra 2.5 mH inductor.

Some harmonics around f_x are aroused because of the poor robustness caused by the typical control. Adding an extra 0.2 mH inductor can make the system unstable and trigger the protection during the start-up in Fig. 13(b). Note that the desired amplitude of the current reference is also set at about 10 A. But the inverter cannot reach the steady-state operation. In other words, even if a small grid impedance exists, the performance with strategy 1 is poor.

Then, the performance with the proposed strategy 2 is tested, and waveforms are shown in Fig. 14. Compared with strategy 1 in Fig. 13, significant improvement is achieved by strategy 2, due to the improved phase margin by the impedance-phase shaping. The current harmonics shown in Fig. 13 have been highly suppressed. Even the grid exhibits a large grid impedance (by adding an extra 2.5 mH inductor), the system works stably, indicating a high robustness.

In addition, as shown in Section VI-A, designing different *LCL* parameters can be beneficial for robustness. With *parameter* 2, Fig. 15(a) shows the waveform with the typical grid current AD without the phase shaping, i.e., strategy 1. Compared with the unstable waveform [see Fig. 13(b)] with *parameter* 1, the inverter works stably without using the phase shaping when the grid impedance is the same. But note that harmonics in the range of 1–2 kHz are aroused because of the poor phase margin. If the grid impedance grows, the protection is triggered by the amplified harmonics during the start-up, similar to that in Fig. 13(b). On the contrary, by applying the phase shaping, the waveform is shown in Fig. 15(b). Harmonics are suppressed due to the improved phases. In Fig. 15(c), even the grid impedance increases to more than 2.5 mH, and the inverter performs satisfactorily. The applicability of the proposed control for different *LCL* parameters has been verified.

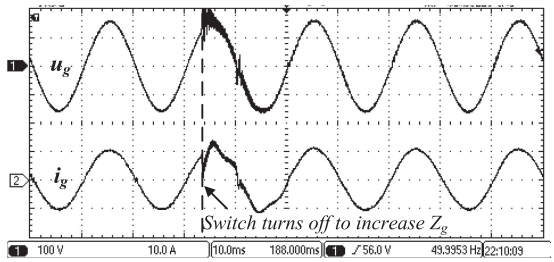

Fig. 16. Waveforms with the proposed control subjected to a sudden increase of grid impedance.

Moreover, the inverter with the proposed strategy 2 is tested when the grid impedance increases suddenly. The 2.5 mH inductor is paralleled with a switch and a snubber. By suddenly turning OFF the switch, Z_g is increased. Waveforms are shown in Fig. 16. Because of the inherent feature of the inductor, the grid current cannot change suddenly and some oscillations are then yielded. After a short time (less than half-grid cycle), the grid current gets smooth again, indicating a high robustness against the wide grid impedance variation.

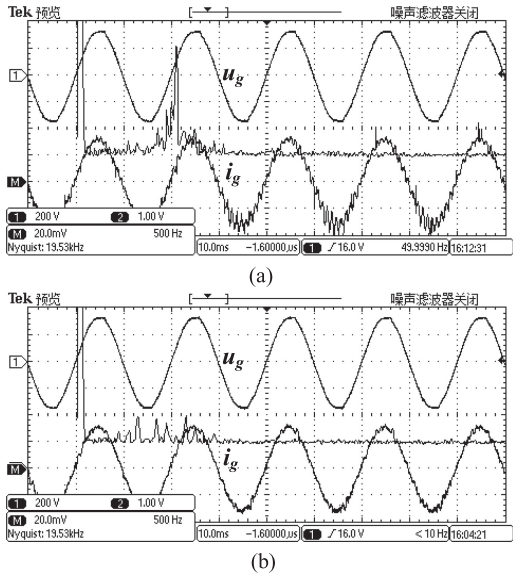

Fig. 17. Waveforms under a commercial grid. (a) strategy 1. (b) Strategy 2.

As long as the merits of the proposal have been successfully verified under the safe and low-voltage condition, it is, thus, reliable to run the proposed control in a real grid-connected application. A transformer-less H5 inverter with *parameter* 2 is directly tied to a commercial 220 V/50 Hz grid. Fig. 17 shows the waveforms with different strategies. Current i_g was measured through a sampling resistor and "1 V" means 10 A. The harmonic spectrum of PCC voltage varied randomly with the change in time, but the measured THD was about 2%. Besides, the real grid impedance was unknown due to the lack of measuring equipment. Under such a random condition, using strategy 1 yielded a large number of harmonics around 1 kHz, but the proposed strategy 2 limited those harmonics. The percentage of the maximum harmonic with strategy 1 was about 5.1%, while that with strategy 2 was about 1.2%.

VIII. Conclusion

The grid current feedback AD requires sampling only of the grid current, but the robustness is endangered by the voltage distortions and the grid impedance variation. By analyzing the limitation of the typical grid current feedback AD, a robust grid current control plus design strategy has been proposed. The conclusions are as follows.

1) The grid current feedback AD without the control delay represents the worst case for stabilizing the system considering the grid impedance. The phase of the inverter output impedance with such AD is close to or below $-90°$ at a specific frequency named f_{peak} (which only relates to *LCL* parameters and is between the bandwidth and the *LCL* resonance frequency). Hence, the contradiction between the high bandwidth and the high robustness is yielded and thus blocks the application.
2) The feedforward of the PCC voltage can enhance the start-up performance and thus should be integrated into the inverter control. But, even in a small grid impedance case, because the phases of the inverter output impedance are considerably reduced, the voltage feedforward can cause the serious instability, which cannot be solved by reducing the bandwidth.
3) In order to enhance the robustness, a novel phase shaping control method for increasing the phases around f_{peak} is proposed and a straightforward design is proposed. Besides, based on increasing the phases at lower frequencies ($< f_{\text{peak}}$), the fundamental PVF and its implementation strategy (including the parameter selection and the start-up procedure) are proposed, and the robust design of the resonant current controller is presented.
4) The results have verified the proposed robust control and the simple and straightforward design in the weak grid application. The minimum start-up inrush current, the low grid current distortion, and the high robustness against the grid impedance variation are achieved by the proposed control with a minimal number of sensors simultaneously.

References

[1] X. Zheng, L. Xiao, Y. Lei, and Z. Wang, "Optimisation of *LCL* filter based on closed-loop total harmonic distortion calculation model of the grid-connected inverter," *IET Power Electron.*, vol. 8, no. 6, pp. 860–868, Jun. 2015.

[2] M. Sanatkar-Chayjani and M. Monfared, "Stability analysis and robust design of *LCL* with multituned traps filter for grid-connected converters," *IEEE Trans. Ind. Electron.*, vol. 63, no. 11, pp. 6823–6834, Nov. 2016.

[3] R. N. Beres *et al.*, "A review of passive power filters for three-phase grid-connected voltage-source converters," *IEEE J. Emerging Select. Topics Power Electron.*, vol. 4, no. 1, pp. 54–69, Mar. 2016.

[4] J. Dannehl, M. Liserre, and F. W. Fuchs, "Filter-based active damping of voltage source converters with *LCL* filter," *IEEE Trans. Ind. Electron.*, vol. 58, no. 8, pp. 3623–3633, Aug. 2011.

[5] Y. Tang, P. C. Loh, P. Wang, F. H. Choo, F. Gao, and F. Blaabjerg, "Generalized design of high performance shunt active power filter with output *LCL* filter," *IEEE Trans. Ind. Electron.*, vol. 59, no. 3, pp. 1443–1452, Mar. 2012.

[6] M. Xue, Y. Zhang, Y. Kang, Y. Yi, S. Li, and F. Liu, "Full feedforward of grid voltage for discrete state feedback controlled grid-connected inverter with *LCL* filter," *IEEE Trans. Power Electron.*, vol. 27, no. 10, pp. 4234–4247, Oct. 2012.

[7] L. Harnefors, X. Wang, A. G. Yepes, and F. Blaabjerg, "Passivity-based stability assessment of grid-connected VSCs—An overview," *IEEE J. Emerging Sel. Topics Power Electron.*, vol. 4, no. 1, pp. 116–125, Mar. 2016.

[8] C. Zou, B. Liu, S. Duan, and R. Li, "Influence of delay on system stability and delay optimization of grid-connected inverters with *LCL* filter," *IEEE Trans. Ind. Informat.*, vol. 10, no. 3, pp. 1775–1784, Aug. 2014.

[9] J. Wang, J. D. Yan, L. Jiang, and J. Zou, "Delay-dependent stability of single-loop controlled grid-connected inverters with *LCL* filters," *IEEE Trans. Power Electron.*, vol. 31, no. 1, pp. 743–757, Jan. 2016.

[10] R. A. Fantino, C. A. Busada, and J. A. Solsona, "Optimum PR control applied to *LCL* filters with low resonance frequency," *IEEE Trans. Power Electron.*, vol. 33, no. 1, pp. 793–801, Jan. 2018.

[11] T. Liu, Z. Liu, J. Liu, Y. Tu, and Z. Liu, "Stability enhancement of single-loop inverter-side current feedback controlled grid-connected inverters with *LCL* filters," in *Proc. IEEE Energy Convers. Congr. Expo.*, Cincinnati, OH, USA, 2017, pp. 3030–3037.

[12] J. Xu, S. Xie, L. Huang, and L. Ji, "Design of *LCL*-filter considering the control impact for grid-connected inverter with one current feedback only," *IET Power Electron.*, vol. 10, no. 11, pp. 1324–1332, Sep. 2017.

[13] Y. Liu, W. Wu, Y. He, Z. Lin, F. Blaabjerg, and H. S. H. Chung, "An efficient and robust hybrid damper for *LCL*- or *LLCL*-based grid-tied inverter with strong grid-side harmonic voltage effect rejection," *IEEE Trans. Ind. Electron.*, vol. 63, no. 2, pp. 926–936, Feb. 2016.

[14] W. Yao, Y. Yang, X. Zhang, F. Blaabjerg, and P. C. Loh, "Design and analysis of robust active damping for *LCL* filters using digital notch filters," *IEEE Trans. Power Electron.*, vol. 32, no. 3, pp. 2360–2375, Mar. 2017.

[15] J. Xu, S. Xie, and T. Tang, "Active damping-based control for grid-connected *LCL*-filtered inverter with injected grid current feedback only," *IEEE Trans. Ind. Electron.*, vol. 61, no. 9, pp. 4746–4758, Sep. 2014.
[16] M. Hanif, V. Khadkikar, W. Xiao, and J. L. Kirtley, "Two degrees of freedom active damping technique for *LCL* filter-based grid connected PV systems," *IEEE Trans. Ind. Electron.*, vol. 61, no. 6, pp. 2795–2803, Jun. 2014.
[17] L. Zhou *et al.*, "Robust two degrees-of-freedom single-current control strategy for *LCL*-type grid-connected DG system under grid-frequency fluctuation and grid-impedance variation," *IET Power Electron.*, vol. 9, no. 14, pp. 2682–2691, Nov. 2016.
[18] X. Wang, F. Blaabjerg, and P. C. Loh, "Grid-current-feedback active damping for *LCL* resonance in grid-connected voltage-source converters," *IEEE Trans. Power Electron.*, vol. 31, no. 1, pp. 213–223, Jan. 2016.
[19] J. Wang, J. D. Yan, and L. Jiang, "Pseudo-derivative-feedback current control for three-phase grid-connected inverters with *LCL* filters," *IEEE Trans. Power Electron.*, vol. 31, no. 5, pp. 3898–3912, May 2016.
[20] T. Liu, Z. Liu, J. Liu, and Z. Liu, "Virtual impedance-based active damping for *LCL* resonance in grid-connected voltage source inverters with grid current feedback," in *Proc. IEEE Energy Convers. Congr. Expo.*, Milwaukee, WI, USA, 2016, pp. 1–8.
[21] M. A. Gaafar, G. M. Dousoky, E. M. Ahmed, and M. Shoyama, "Systematic design of grid-current-based active damping for grid-connected *LCL* filters," in *Proc. IEEE Appl. Power Electron. Conf. Expo.*, Tampa, FL, USA, 2017, pp. 2652–2657.
[22] W. Wu *et al*., "An improved active damping method with grid-side current feedback to maximize damping ratio for *LCL*-type grid-connected inverter," in *Proc. IEEE Energy Convers. Congr. Expo.*, Cincinnati, OH, USA, 2017, pp. 5607–5611.
[23] C. A. Busada, S. Gomez Jorge, and J. A. Solsona, "Full-state feedback equivalent controller for active damping in *LCL*-filtered grid-connected inverters using a reduced number of sensors," *IEEE Trans. Ind. Electron.*, vol. 62, no. 10, pp. 5993–6002, Oct. 2015.
[24] R. Guzman, L. Garcia de Vicuna, J. Morales, M. Castilla, and J. Miret, "Model-based active damping control for three-phase voltage source inverters with *LCL* filter," *IEEE Trans. Power Electron.*, vol. 32, no. 7, pp. 5637–5650, Jul. 2017.
[25] M. Liserre, R. Teodorescu, and F. Blaabjerg, "Stability of photovoltaic and wind turbine grid-connected inverters for a large set of grid impedance values," *IEEE Trans. Power Electron.*, vol. 21, no. 1, pp. 263–272, Jan. 2006.
[26] J. Sun, "Impedance-based stability criterion for grid-connected inverters," *IEEE Trans. Power Electron.*, vol. 26, no. 11, pp. 3075–3078, Nov. 2011.
[27] M. Castilla, J. Miret, J. Matas, L. García de Vicuña, and J. M. Guerrero, "Control design guidelines for single-phase grid-connected photovoltaic inverters with damped resonant harmonic compensators," *IEEE Trans. Ind. Electron.*, vol. 56, no. 11, pp. 4492–4501, Nov. 2009.
[28] G. Shen, X. Zhu, J. Zhang, and D. Xu, "A new feedback method for PR current control of *LCL*-filter-based grid-connected inverter," *IEEE Trans. Ind. Electron.*, vol. 57, no. 6, pp. 2033–2041, Jun. 2010.
[29] W. Li, X. Ruan, D. Pan, and X. Wang, "Full-feedforward schemes of grid voltages for a three-phase *LCL*-type grid-connected Inverter," *IEEE Trans. Ind. Electron.*, vol. 60, no. 6, pp. 2237–2250, Jun. 2013.
[30] J. Xu, S. Xie, and T. Tang, "Evaluations of current control in weak grid case for grid-connected *LCL*-filtered inverter," *IET Power Electron.*, vol. 6, no. 2, pp. 227–234, Feb. 2013.
[31] M. Cespedes and J. Sun, "Impedance modeling and analysis of grid-connected voltage-source converters," *IEEE Trans. Power Electron.*, vol. 29, no. 3, pp. 1254–1261, Mar. 2014.
[32] D. Yang, X. Ruan, and H. Wu, "Impedance shaping of the grid-connected inverter with *LCL* filter to improve its adaptability to the weak grid condition," *IEEE Trans. Power Electron.*, vol. 29, no. 11, pp. 5795–5805, Nov. 2014.
[33] X. Chen, Y. Zhang, S. Wang, J. Chen, and C. Gong, "Impedance-phased dynamic control method for grid-connected inverters in a weak grid," *IEEE Trans. Power Electron.*, vol. 32, no. 1, pp. 274–283, Jan. 2017.
[34] J. Xu, S. Xie, and T. Tang, "Improved control strategy with grid-voltage feedforward for *LCL*-filter-based inverter connected to weak grid," *IET Power Electron.*, vol. 7, no. 10, pp. 2660–2671, Oct. 2014.
[35] D. Yang, X. Ruan, and H. Wu, "A real-time computation method with dual sampling modes to improve the current control performances of the *LCL*-type grid-connected inverter," *IEEE Trans. Ind. Electron.*, vol. 62, no. 7, pp. 4563–4572, Jul. 2015.
[36] J. Xu, S. Xie, and B. Zhang, "Stability analysis and improvement of the capacitor current active damping of the *LCL* filters in grid-connected applications," *J. Power Electron.*, vol. 16, no. 4, pp. 1565–1577, Jul. 2016.
[37] C. Chen, J. Xiong, Z. Wan, J. Lei, and K. Zhang, "A time delay compensation method based on area equivalence for active damping of an *LCL*-type converter," *IEEE Trans. Power Electron.*, vol. 32, no. 1, pp. 762–772, Jan. 2017.
[38] M. Ciobotaru, R. Teodorescu, and F. Blaabjerg, "A new single-phase PLL structure based on second order generalized integrator," in *Proc. 37th IEEE Power Electron. Spec. Conf.*, 2006, pp. 1–6.
[39] X. Wang, F. Blaabjerg, and P. C. Loh, "Virtual RC damping of *LCL*-filtered voltage source converters with extended selective harmonic compensation," *IEEE Trans. Power Electron.*, vol. 30, no. 9, pp. 4726–4737, Sep. 2015.
[40] Z. Xin, P. C. Loh, X. Wang, F. Blaabjerg, and Y. Tang, "Highly accurate derivatives for LCL-filtered grid converter with capacitor voltage active damping," *IEEE Trans. Power Electron.*, vol. 31, no. 5, pp. 3612–3625, May 2016.

Jinming Xu (S'13–M'18) was born in Jiangsu Province, China, in 1987. He received the B.S. degree in electrical engineering and the Ph.D. degree in power electronics from Nanjing University of Aeronautics and Astronautics (NUAA), Nanjing, China, in 2009 and 2017, respectively.

In 2017, he joined the College of Automation Engineering, NUAA, where he is currently a Lecturer. He has authored and coauthored more than 30 technical papers in many international journals and conference proceedings. His current research interests mainly include the grid-connected inverters and control strategies, and renewable power generations.

Dr. Xu was a recipient of the 2015 IET Power Electronics Premium Award.

Shaojun Xie (M'05) was born in Hubei Province, China, in 1968. He received the B.S., M.S., and Ph.D. degrees in electrical engineering from Nanjing University of Aeronautics and Astronautics (NUAA), Nanjing, China, in 1989, 1992, and 1995, respectively.

In 1992, he joined the Faculty of Electrical Engineering Teaching and Research Division, NUAA, where he is currently a Professor with the College of Automation Engineering. In recent five years, he has authored and coauthored more than 100 technical papers published in many international journals and conference proceedings. His main research interests include the aviation electrical power supply and power electronic conversion.

Dr. Xie was a recipient of the 2015 IET Power Electronics Premium Award.

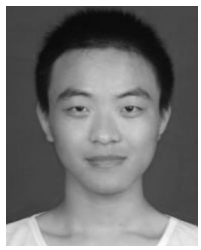

Binfeng Zhang (S'16) was born in Jiangsu, China, in 1991. He received the B.S. degree in electrical engineering in 2013 from Nanjing University of Aeronautics and Astronautics, Nanjing, China, where he is currently working toward the Ph.D. degree.

His current research interests mainly include the grid-connected inverter and application of wide bandgap devices.

Qiang Qian (S'15) was born in Anhui, China, in 1992. He received the B.S. degree in electrical engineering in 2012 from Nanjing University of Aeronautics and Astronautics, Nanjing, China, where he is working toward the Ph.D. degree in electrical engineering.

His current research interests include the modeling and the control of the multiparallel grid-connected inverters.